Investigation of field electron emission from ITO/glass interfaces

JADWIGA OLESIK*
Institute of Physics, Jan Dlugosz University of Czestochowa, al. Armii Krajowej 13/15, 42-201 Czestochowa, Poland

In this work, the electron emission properties from thin, doped In_2O_3 and SnO_2 layers (ITO) have been studied. The films of thickness from 10 nm to 300 nm were deposited on a glass substrate and exposed to the electric field and UV light. The studied emission phenomena were: the field induced secondary electron emission (FISE), the field induced electron emission (FIEE) and the field induced photoemission (FIPE). Electric field inside the emitter was found to be of the order of 1 MV/m. The FISE phenomenon is based on the Malter effect. Among others, field modification of the secondary electron spectra has been observed. The FIEE and FIPE measurements relied on determination and analysis of voltage pulse amplitude spectra from a photomultiplier. The emission yield and the electron energy distributions as a function of field intensity in the emitter, the ITO thickness and the UV illumination have been determined. A phenomenological model of the investigated phenomena has been suggested which includes four types of emission mechanisms: an ordinary one (induced exclusively by electric field) and another caused mainly by the surface, volume and tunnel effects.

(Received March 8, 2012; accepted April 11, 2012)

Keywords: ITO, Photoemission, Field effect, Emission yield

1. Introduction

In 1936 Louis Malter studied the phenomenon of secondary emission from poorly conducting oxides and discovered some anomalies [1–3]. The anomalous secondary emission was caused by charging of the emitter surface and production of an internal electric field in investigated samples. Uncontrolled behavior of this emission made impossible practical application of its properties like e.g. some high values of the secondary emission coefficient. If it was possible to produce a given value internal field in a sample, then the secondary emission would be controllable. In this work such an attempt has been taken.

On the glass slide surface we deposited a conducting film of ITO (indium tin oxide). On the other side, NiCr alloy was deposited as the electrode used for biasing by negative voltage. Such a capacitor like structure allowed to create an internal electric field. The field direction favoured the electron release from the ITO into the vacuum. By application of a given value of the field, the electron emission intensity was controlled. Primarily this method was used in the study of the secondary electron emission (FISE).

It was found that the results, similar to the Malter emission, significantly differed from commonly known [4]. In further studies, the secondary electron beam was switched off. In this way, the influence of exclusively electric field on the process of electron heating, thus on their emission into the vacuum, was investigated. Additionally we could illuminate the ITO layers by UV light and study an intensity of the field induced electron emission (FIEE) and photoemission (FIPE). The investigated emitting films were made of doped SnO_2 and In_2O_3, which are materials conducting the current and transparent to the light. The films, commonly called ITO layers, find numerous applications in optoelectronics [5–11]. The ITO-glass interfaces are promising materials for optoelectronic and nonlinear optics and these features are determined by the nano-interfaces effectively interacting with the phonon sub-system [12–13].

2. Samples and apparatus

For preparation of the samples, we used 0.2 nm-thick glass slides which were covered on one side with conducting ITO films of thickness in the range from 10 nm to 300 nm. Deposition was made by direct current reactive ion sputtering [14]. In_2O_3 films were doped with tin, whereas SnO_2 films with antimony. The sputtering target was an alloy: either indium (90%) and tin (10%) or tin (93%) and antimony (7%) [15,16]. The ITO film was the emitting surface, whereas the other layer of 1 μm-thick NiCr was biased by a negative voltage (field electrode). Surface resistance R_s of ITO films was in the range $8 \cdot 10^4$ Ω/□ to $3 \cdot 10^2$ Ω/□. The film thickness was measured by a Talysurf 4 profilometer [17]. The investigated samples have a MIS type structure: field electrode-glass-ITO, as shown in Fig. 1.

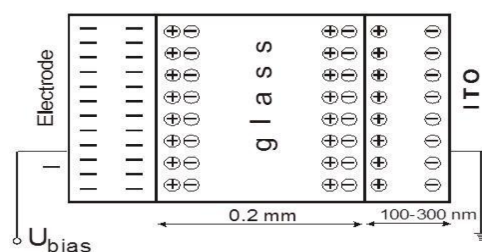

Fig. 1. Shape of a sample and the charge distribution under biasing.

A scheme of the electric set used to study the field induced secondary emission (FISE) is presented in Fig. 2a. The internal electric field in the sample was generated by high voltage power supply, which allowed a negative biasing voltage to be applied to the rear side of the sample. The primary electron beam was changed from 25 eV to 200 eV. Secondary electrons from the sample were directed to the energy electron analyser. A four-grid retarding potential analyser makes it possible to investigate change in the secondary emission coefficient when all the grids are short circuited and grounded. To obtain the electron energy distribution, the negative potential U_a relatively to the emitting surface of the sample is applied to the analysing grids.

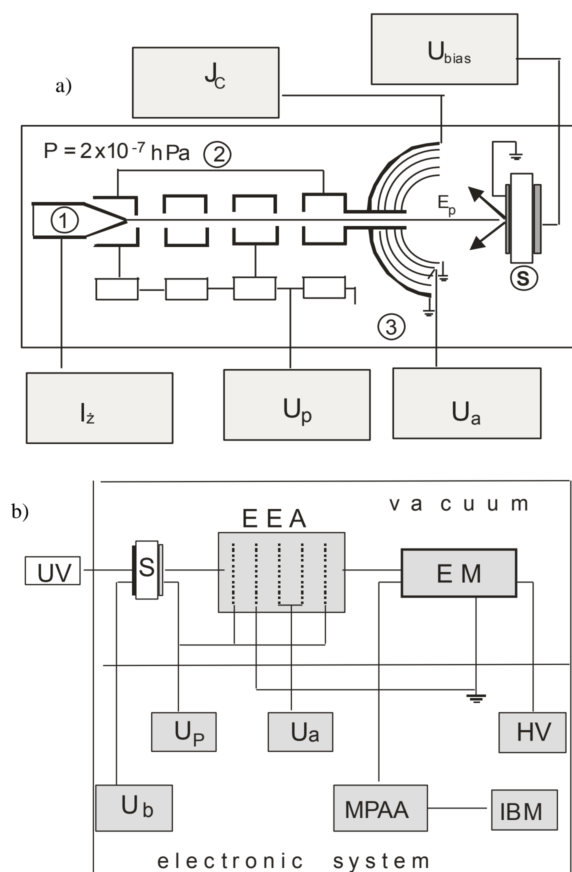

Fig. 2. Experimental setup used to study of a) the field induced secondary emission (FISE), b) the field induced electron emission (FIEE). 1–electron gun, 2–accelerating system, 3–four-grid retarding potential analyzer, S–sample, U_p–accelerating voltage, U_a–analysing voltage, J_c–collector voltage, U_b–biasing voltage, E_p–primary electron energy, UV–quartz lamp, EEA–energy electron analyzer, EM–electron multiplier (channeltron), HV–high voltage switch, (2.9 kV), MPAA–multichannel pulse amplitude analyzer, IBM–computer.

In order to minimise the Malter effect and accompanying it charging of the sample surface as a result of primary electron bombarding, it was decided to investigate only field induced electron emission, i.e. without participation of a primary beam. The schematic diagram of the apparatus used to study the field induced electron emission (FIEE) is shown in Fig. 2b. Applying biasing voltage U_{bias}, from the interval from –2 kV to 0 V to the field electrode creates an internal field, which favour electron emission into vacuum. Appropriate operational conditions for the electron multiplier were received by acceleration of electrons between the emitting film and the multiplier, i.e. voltage U_p = –200 V at the emitting film and grounded entrance of the multiplier (EM). Depending on the kind of performed measurements, grids 3 and 4 of the electron energy analyser (EEA) were either grounded or polarized by negative analysing voltage U_a. The electrons accelerated to the energy eU_p create voltage pulses in the multiplier. These pulses are recorded in the multichannel pulse amplitude analyser (MPAA). The multiplier is joined to preamplifier, which adjusts its parameters to MPAA. The multichannel analyser registers pulses, which are amplified. The pulses are recorded according to their height, creating so-called voltage pulse amplitude spectrum. The amplitude spectra (for various U_{bias}) were measured for unilluminated samples and samples illuminated by a quartz lamp (UV).

3. Results

3. 1. Field induced secondary emission (FISE)

Using the equipment shown in Fig. 2a, the collector current intensity I_c as a function of the primary electron energy E_p (U_{bias}=const) was measured and after performing some calculations was presented as δ = f(E_p), (Fig. 3). When the energy E_p is a parameter, then the dependence of I_c on U_{bias} can be derived and further calculated over to the dependence δ = f(U_{bias}) (Fig. 4).

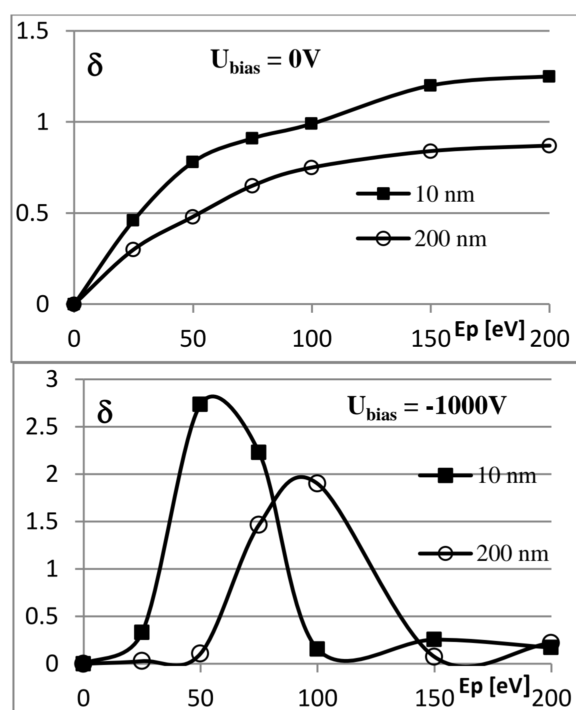

Fig. 3. Dependences of the coefficient δ on E_p for a 10 and 200 nm thick ITO film; U_{bias}=0V and U_{bias}= –1 kV.

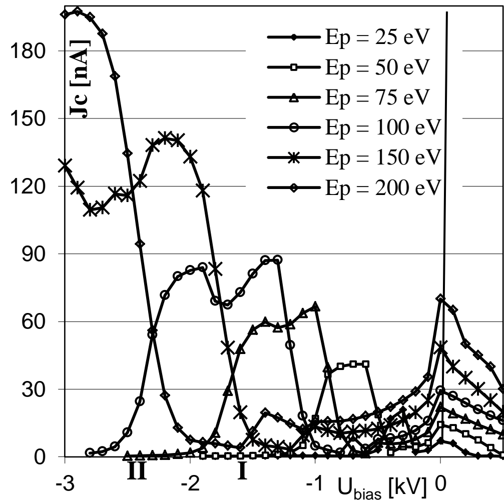

Fig. 4. Dependences of the collector current J_C on U_{bias} for a different values of E_p (I–I_{max}, II–II_{max}).

It is known, that secondary emission coefficients δ_0 (without field) for semiconductors are greater than 1 but there are no data in the literature for coefficients δ (with field). As one can see in Figs. 3 and 4, values of the coefficients δ depend on the energy E_p, U_{bias} voltage and ITO thickness. Due to the limited range of E_p (primary beam energy), it was impossible to obtain the highest value of δ for an unbiased sample [4].

In Fig. 4 we can see that the curves $\delta = f(U_{bias})$ are non-monotonic and have two distinct maxima denoted as I_{max} (at lower U_{bias}) and II_{max} (at higher U_{bias} value). With increasing E_p, the maxima move towards higher values of U_{bias}. At higher E_p it was sometimes impossible to obtain II_{max} on the $\delta = f(U_{bias})$ curve, as a result of high U_{bias} and eventual electric discharge. The shape of $\delta = f(E_p)$ at $U_{bias} \neq 0$ is characteristic for a given value of U_{bias} and depends on the thickness of the ITO film. In general, one has to increase E_p with increasing negative U_{bias} in order to maintain the optimum conditions for maximum secondary emission. The thinner ITO layer, the more sensitive is the sample to the external electric field.

Aiming to study the internal electric field influence on concentration of conduction electrons in the close to the surface region, we analyzed energy spectra at various U_{bias} and energy E_p. The energy spectra were obtained using the retarding field method. The spectra for a 200 nm sample at energy E_p = 75 eV: U_{bias}= –800 V (I_{max} of $\delta(U_{bias})$) and U_{bias}= –1.5 kV (II_{max} of $\delta(U_{bias})$) are shown in Fig. 5.

Analysis of the secondary electron energy spectra can be summarized as follows:

- in minimum $\delta = f(U_{pol})$ becomes smaller or even the primary peak disappears,
- in maximum I – the primary peak appears again, is bigger than the secondary peak and shifted towards the lower energy $E < E_p$ (Fig. 5a),
- in maximum II – the elastic peak returns to its previous position and some high energy electrons of energy $E > E_p$ are detected (Fig. 5b),
- in the region outside of maximum II the primary peak and the whole spectrum disappear, similar as it is in the range of U_{bias} corresponding to the minimum in the curve $\delta = f(U_{bias})$.

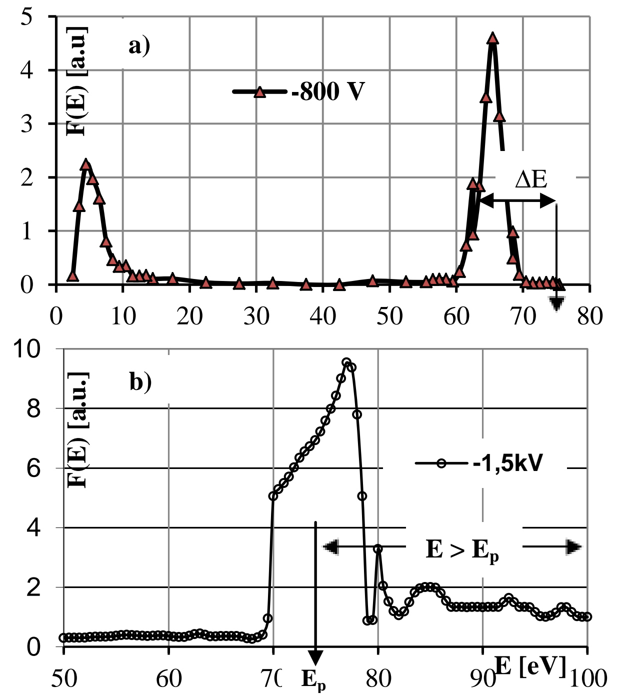

Fig. 5. Energy spectra of secondary electrons for E_p = 75 eV, a) I_{max} of $\delta = f(U_{pol})$, b) II_{max} of $\delta = f(U_{pol})$, ΔE is the primary peak shift.

3.2. Field and optically induced electron emission (FIEE and FIPE)

Exemplary voltage pulse amplitude spectra for the ITO 100 nm films (for some chosen U_{bias} values both with and without UV illumination) are shown in Fig. 6. Number of pulses per unit time, i.e. the frequency of counts n, increases exponentially with increasing U_{bias}, as shown in Fig. 7. The increase is several times greater at UV illumination, but it differs for films of various thicknesses [18,19].

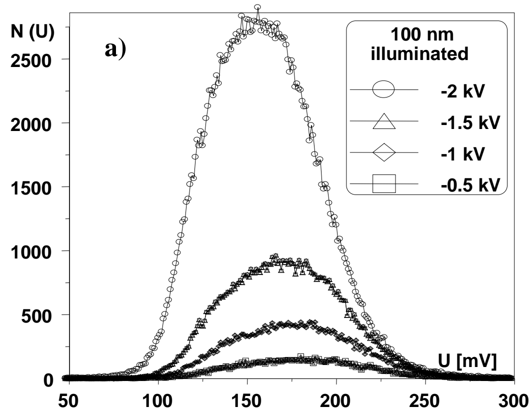

Fig. 6a. Voltage pulse amplitude spectra under illumination at some chosen voltages U_{bias}.

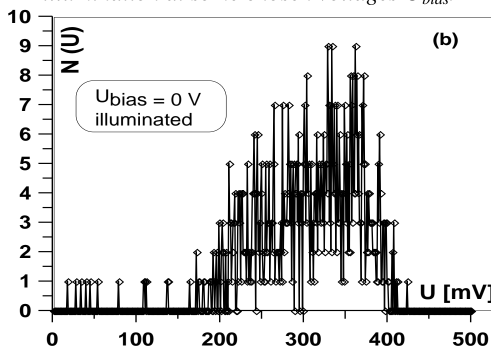

Fig. 6b. Voltage pulse amplitude spectra for photoeffect at $U_{bias} = 0$.

In general, the thinner ITO films the greater emission efficiency. It was experimentally established that functional dependences of n on $U_{\rm bias}$ for the ITO layers of various thickness are as follows:

- for 200 nm: $n = a(U_b)^{3/2}$, (without illum), $n = a_1\exp(a_2U_b)$, (illum.),
- for 100 nm: $n = b_1\exp(kU_b)$ (without illum.), $n = b_2\exp(kU_b)$, (illum.),
- for 10 nm: $n = c_1(U_b)^5$ (without illum.), $n = c_2(U_b)^6$ (illum.).

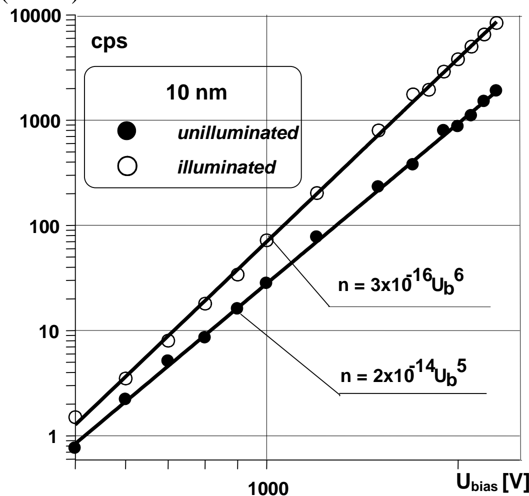

Fig. 7. Count frequency n as a function of voltage U_{bias} (U_b) for a sample with 10 nm thick ITO layer.

The FIEE or FIPE behavior according to the equation of the type $n \sim \exp(aU_{\rm bias})$ can be compared to the mechanism of self-contained discharge (so called Townsend current) in rarefied gasses and also to the Malter electron avalanche in porous emitters [3].

Energy of electrons emitted from ITO films was studied with the well known method of a retarding field [3, 4]. At first, the amplitude spectra for several analyzing voltages $U_{\rm a}$ at constant $U_{\rm bias}$ were measured. Then for each value of $U_{\rm a}$, the frequency n was determined. It is evident that the frequency n in the particular analyzer channels should decrease with increasing negative $U_{\rm a}$. After differentiation of the obtained retarding curves $n = f(U_{\rm a})$, the energy distributions $F(E) = f(E)$ were obtained. An exemplary energy spectrum for the 10 nm-thick sample at biasing voltage $U_{\rm b} = -1$ kV is shown in Fig. 8.

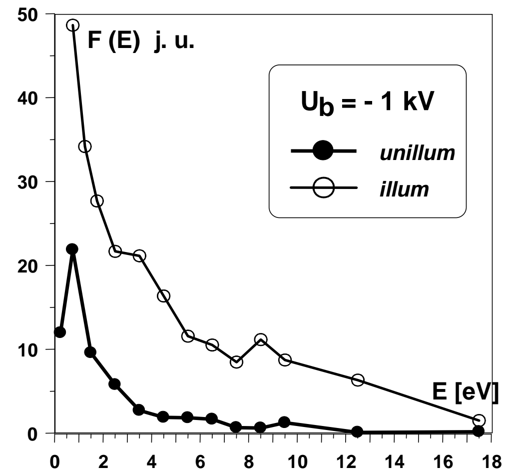

Fig. 8. Energy spectra of electrons and photoelectrons for a sample with 10nm thick ITO layer, $U_{bias} = -1$ kV.

The energy analysis reveals that about 80 % of emitted electrons have energy less than 10 eV. This energy decreases with increasing $U_{\rm bias}$ which is connected with increasing number of emitted electrons. This effect is caused by electron collisions leading to significant energy losses in the region of enhanced electron concentration near the surface.

4. Discussion

The investigated system is a structure similar to a capacitor with a dielectric. Charge distribution in the system is shown in Fig. 9. In the ITO layer there are created two zones of different electron concentration: depleted at the glass surface and enhanced at the vacuum boundary. The voltage $U_{\rm bias}$ is distributed in glass (U_g) and semiconductor (U_I) as follows:

$$U_{bias} = U_g + U_I \quad (1)$$

where: $U_g = \frac{Q}{C_g}$, $U_I = \frac{Q}{C_I}$

The capacities C_g and C_l are:

$$C_g = \frac{\varepsilon_o \varepsilon_g}{d}, \quad C_I = \frac{\varepsilon_o \varepsilon_I}{D}, \tag{2}$$

where: $D = \sqrt{\frac{kT\varepsilon_o\varepsilon_I}{n_o e^2}}$, n_o–concentration of charge carriers.

The capacity C_l is related to the region of charge volume in the ITO layer. The magnitude of C_l depends on the width of the depleted zone i.e. on the U_{bias} voltage. The final capacity of the system is a series connection of C_g and C_l. Assuming that $d = 2\times10^{-4}$ m (glass thickness), $D \le 2\times10^{-7}$ m (ITO thickness), $\varepsilon_g = 10$ and $\varepsilon_I < \varepsilon_g$, one can calculate, from eqns (1) and (2), the relation between the voltages applied to glass and to semiconductor:

$$C_g = 2\times10^{-3}\, C_I\,;\; U_I = 2\times10^{-3}\, U_g \tag{3}$$

In order to evaluate the electric field intensity in glass and semiconductor one has to take e.g. $U_{bias} = -1$ kV, U_g and U_l according to (3) are: $U_g = 998$ V, $U_l = 2$ V, and finally obtain E_g and E_l:

$$E_g = \frac{U_g}{d} \approx 5\cdot10^6\,\frac{V}{m}, \quad E_I = \frac{U_I}{D} \approx 10^7\,\frac{V}{m} \tag{4}$$

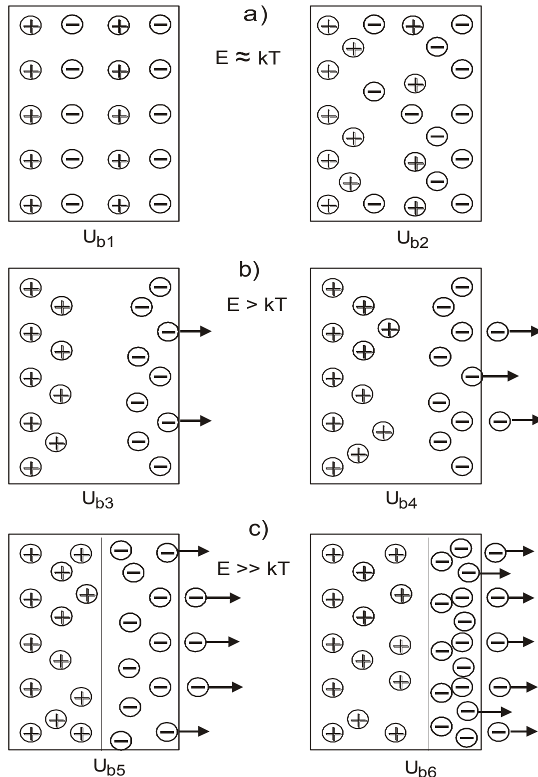

Fig. 9. Schematic illustration of the polarization of ITO layer at various U_{bias}: $U_{b1} < U_{b2} < U_{b3} < U_{b4} < U_{b5} < U_{b6}$, a) $E \approx kT$, b) $E > kT$, c) $E >> kT$

At first, for lower U_{bias} we could not observe distinct depleted and enhanced zones in the ITO film (Fig. 9a). As long as the energy gained by an electron is of the kT order, emission to the vacuum is not possible.

At increased U_{bias}, the energy gained in an electric field is higher than the thermal energy i.e. E > kT (Fig. 9b). The electron can overcome surface potential barrier. Work function for the tin indium oxides is 4.6 eV but at bias conditions it is lower and favours electron emission into the vacuum. In the case of FISE emission, the efficiency can be even lower than under biasing, as a result of electron collisions proceeding in the enhanced zone (minima in Fig. 4). In FIEE the voltage U_{bias} of the order 0.5 kV is sometimes (depending on ITO thickness) enough to observe an electron emission (Fig. 6). With increasing U_{bias} the emission efficiency is exponentially growing, as shown in Fig. 7. Under illumination, the ITO film emits photoelectrons without electric field induction ($U_{bias} = 0$), as shown in Fig. 6b. The electron energy in FISE and FIEE phenomena reaches 10 eV (Fig. 8).

At high U_{bias} values (e.g above 1 kV), conditions corresponding to $E >> kT$ are established in the semiconductor (Fig. 9c). This denotes that:

– two distinct zones (depleted and enhanced) are formed in the ITO film,
– in the depleted zone conditions are favourable for electron acceleration to the energy above the vacuum level (hot electrons, I_{max} in Fig. 4)
– the enhanced zone becomes thinner and electron concentration becomes higher which enables the Zener or tunnel effects to occur (II_{max} in Fig. 4).

In the case of FISE we can observe some field modification of energy spectra:

– shift of the primary peak (Fig. 5a) which is a result of electron energy loss in the enhanced zone,
– appearance of electrons with $E > E_p$ (Fig. 5b) i.e. such primary electrons which did not experience energy loss but gained some energy in the depleted zone and went through it in a tunnel effect.

It is known [20] that the ITO layers have a cluster like structure characterized by a distribution of tiny highly conducting grains separated by thin dielectric layers [21, 22]. These clusters can have additional charge. The ITO film structure depends on a kind of substrate [23]. On a glass substrate, the film grows in two dimensions creating micro grains of the same orientation. It was shown by electron microscopy that ITO films are to some extent porous with defects and channels in a nanometer scale [24–26]. The main defects are oxide vacancies and interstitial dopant ions. Any surface vacancies, pores or volume vacancies can be a source of high local electric fields ($E > 10^7$ V/m). Such fields can initiate a process of avalanche electron multiplication.

In view of these assumptions, electron emission into the vacuum can be described by some mechanisms based on structural defects, as shown in Fig. 10. An ordinary emission is an outcome of hot electrons which gained energy in an electric field. The emission initiated by charged defects on the surface or inside the layer is called the emission induced by a surface or volume vacancies.

The emission resulting from avalanche processes has its origin in lossless channels of a nanometer scale.

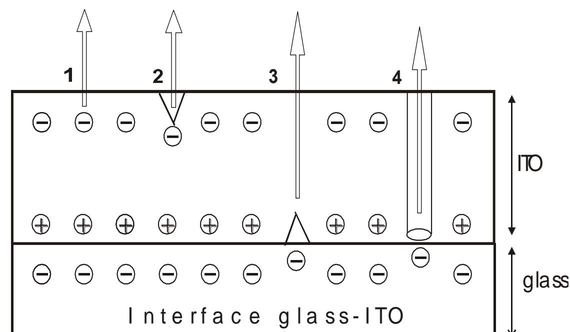

Fig. 10. Probable mechanisms of FIEE phenomenon: 1–normal emission, 2–surface vacancy, 3–bulk defect, 4–tunnel effect.

5. Conclusion

In the systems of glass-ITO type, the following phenomena have been detected and studied: the field induced secondary emission (FISE), the field induced electron emission (FIEE) and the field induced photo emission (FIPE). Anomalous secondary emission effects in the ITO films can be explained by a phenomenological model of two zones with depletion and enhancement of charge carriers. It shows the following anomalies:

– non monotonic behavior of $\delta = f(U_{bias})_{Ep=const}$, and $\delta = f(E_p)_{Ubias=const}$
– field modification of the secondary electron energy spectra.

The FIEE phenomenon relays on the extortion of electron emission due to the electric field in the glass-ITO emitter and proceeds in the fields of the order of 1 MV/m. The electron yield in FIEE and FIPE depends on the field intensity (U_{bias}) inside the emitter, the ITO thickness and it grows non-monotonically with increasing U_{bias}. The energy of emitted electrons does not exceed 10 eV.

The phenomenological model of emission phenomena taking into account 4 types of volume mechanisms of emission has been proposed. The model is in agreement with the mechanism of self-sustained Malter emission.

References

[1] L. Malter, Phys. Rev. **50**, 48 (1936).
[2] M. P. Lorikyan, R. L. Kavalov, N. N.Trofimchuk, JETP Letters **16**, 226 (1972).
[3] I. M. Bronsztein, B. S. Frajman, Wtoricznaja elektronnaja emissija, Moskwa, 1969.
[4] J. Olesik, B. Całusiński, Thin Solid Films **238**, 271 (1994).
[5] I. L. Vossen, Physics of Thin Films, Academic Press, New York, 1977.
[6] K. L. Chopra, S. Major, D. K. Pandya, Thin Solid Films **102**, 1 (1983).
[7] C. G. Granqvist, Handbook of Inorganic Electrochromic Materials, Elsevier, Amsterdam, 1995.
[8] P. S. Monk, R. J. Mortier, D. R. Rosseinsky, Electrochromisms: Fundamental and Applications, VCH, Weinheim, 1995.
[9] C. G. Granqvist, A. Azens, J. Isidorsson, M. Kharrazi, K. Kullman, T. Lindström, G. A. Niklasson, C. G. Ribbing, D. Rönnow, M. S. Mattsson, M. Veszelei, J. of Non-Cryst. Solids **218**, 273 (1997).
[10] R. G. Gordon, MRS Bulletin **25**, 52 (2000).
[11] F. Zhu, K. Zhang, E. Guenther, C. S. Jin, Thin Solid Films **363**, 314 (2000).
[12] I. V. Kityk, J. Ebothe, R. Miedzinski, M. Addou, H. Sieder, A. Karafiat. Semiconductor Science Technology, **18**, 549 (2003).
[13] I. V. Kityk, J. Ebothé, A. El Hichou, B. El Idrissi, M. Addou, J. Krasowski, Journ. of Optics A: Pure and Applied Optics, **5**, 61 (2003).
[14] T. Karasawa, Y. Miyata, Thin Solid Films **223**, 135 (1993).
[15] M. Chen, Z. L. Pei, C. Sun, J. Gong, R. F. Huang, L. S. Wen, J. of Mat. Scien. Letters **19**(2), 99 (2000).
[16] J. George, C. S. Menon, Surface and Coatings Technology **132**(1), 45 (2000).
[17] K. Zakrzewska, E. Leja, Vacuum **36**(7-9), 485 (1986).
[18] J. Olesik, Proc of SPIE **4406**, Ed. G. Kissinger, p. 232 (2001).
[19] J. Olesik, Z. Olesik, Solid-State Electronics **46**, 1913 (2002).
[20] N. Mott, Metal-Insulator Transitions, Taylor & Francis London, 1990.
[21] S. P. Harvey, T. O. Mason, Y. Gassenbauer, R. Schafranek, A. Klein, J. of Phys. D: App. Phys. **39**(18), 3959 (2006).
[22] J. Ederth, P. Heszler, A. Hultåker, G. A. Niklasson, C. G. Granqvist, Thin Solid Films **445**(2), 199 (2003).
[23] M. Purica, F. Iacomi, C. Baban, P. Prepelita, N. Apetroaei, D. Mardare, D. Luca, Thin Solid Films **515**, 8674 (2007).
[24] J. Ederth, G. A. Niklasson, A. Hultåker, P. Heszler, C. G. Granqvist, Appl. Phys. **93**(2), 984 (2003).
[25] G. B. Gonzalez, T. O. Mason, J. P. Quintana, O. Warschkow, D. E. Ellis, J-H. Hwang, J. P. Hodges, J. D. Jorgensen, J. of Appl. Phys. **96**(7), 3912 (2004).
[26] J. Ederth, A. Hultåker, G. A. Niklasson, P. Heszler, A. R. van Doorn, M. J. Jongerius, D. Burgard, C. G. Granqvist, Appl. Phys. A **81**(7), 1363 (2005).

*Corresponding author: j.olesik@ajd.czest.pl